PHYSICAL REVIEW B VOLUME 17, NUMBER 11 1 JUNE 1978

Molecular-dynamics study of the classical Ising model in a transverse field

P. Prelovšek*
Physik-Department der Technischen Universität München, 8046 Garching, West Germany

I. Sega
J. Stefan Institute, University of Ljubljana, 61001 Ljubljana, Yugoslavia
(Received 29 December 1977)

The molecular-dynamics technique is applied to the study of the classical ($S = \infty$) Ising model in a transverse field on a simple-cubic lattice. The results for the longitudinal- and transverse-relaxation shape function are presented for a set of temperatures in the disordered phase at one value of the transverse field. The longitudinal spectra at $T = \infty$ and in the critical regime are analyzed via the Mori's continued-fraction expansion and compared with various approximate results within this approach. The relation of the observed central mode to a domain-wall motion is also discussed. However, due to heavy-damping phenomena no well-defined propagating modes are observed in the critical region. Finally, transverse correlation functions are tested against their diffusive character.

I. INTRODUCTION

The Ising model in a transverse field (IMTF) has been in the past decade extensively studied in connection with a variety of physical systems like KH_2PO_4 (KDP)-type hydrogen-bonded ferroelectrics, cooperative Jahn-Teller systems, rare-earth compounds with a singlet crystal-field ground state, etc.[1] Recent theoretical investigations were devoted predominantly to the dynamics of the model, where the emphasis was put on its critical regime. To improve over the conventional random-phase approximation (RPA) results, which lack the damping of the modes and are therefore not able to cope with heavy-damping effects in real situations, Chock and Dagonnier[2] as well as Moore and Williams[3] derived a set of kinetic equations for the spin-correlation functions which they solved numerically. In the critical region, Mori's continued-fraction analysis, as applied to the relaxation shape functions in the IMTF,[4,5] seems to be more rewarding. By this method one is able to extract the low-frequency phenomena in a systematic way, but at a cost of introducing rather phenomenological parameters at a certain level. Nevertheless, the qualitative and the quantitative agreement of these multipole approximations, as they are often referred to, with the actual IMTF spectra, still remain to be tested.

Recently, there have also appeared speculations on the low-frequency dynamics of the IMTF, stimulated by the numerical-simulation work of Schneider and Stoll[6] on the lattice-dynamical model for the structural phase transitions. The authors presented evidence of a central peak in the critical regime above the transition temperature, which was characterized by two essential features: (a) in a substantial range of temperatures $T > T_c$ the central peak remained well separated from the underdamped soft mode, (b) for small wave vectors $\vec{q}$ it split up into a double-peak structure, giving rise to a new excitation branch. The central peak and the new branch were attributed to the propagating domain walls. Due to the physically apparent relationship between the IMTF and the lattice-dynamical model, one is tempted to expect similar kind of phenomena also in the IMTF.

In order to clarify these points by objective means we performed a molecular dynamics (MD) study of the IMTF on a three-dimensional (3-D) simple cubic lattice. As the quantum case $S = \frac{1}{2}$ cannot be approached by a simulation method, due to an enormous number of basic states for any reasonable system, we had to rely on the classical ($S = \infty$) version of the model. Although the $S = \frac{1}{2}$ case basically differs from the $S = \infty$ IMTF (CIMTF) in its physical nature at low temperatures, it is reasonable to expect that both reproduce similar qualitative features for $T > T^*$, T^* being the quantum to classical crossover temperature of the $S = \frac{1}{2}$ model. At least two arguments could be put forward in support of this conjecture: (a) Moment-expansion results on the Heisenberg-model dynamics for an arbitrary value S indicate that there is an almost complete qualitative as well as a quantitative agreement between the results for various S, if the variables as the frequency and the interaction are properly rescaled[8]; (b) the static[9] and the dynamic critical behavior[10] are expected to remain in the same universality class for all spin values S, at least in the region where the IMTF retains an Ising-type character, i.e., below the critical transverse field. Recent Monte Carlo (MC) simulation results for

the CIMTF statics, obtained by the present authors,[11] also support this similarity.

The organization of the paper is as follows: In Sec. II we introduce the model and derive, following Mori's continued-fraction analysis, the three-pole and the two-pole approximations for the relaxation shape functions. In Sec. III some technical details of our MD simulation as well as our method of MD data analysis are described. Section IV is devoted to the presentation and the discussion of our results. First, the $T=\infty$ longitudinal relaxation spectra are shown and analyzed in connection with the three-pole and the two-pole approximations. In the finite-temperature examples, which are located in the critical regime, the longitudinal functions are tested with respect to a presumable new excitation branch within the central mode. Again, a comparison with the continued-fraction analysis results is performed and a quantitative evaluation of the phenomenological parameters entering the three-pole approximation is carried out. Finally, we discuss the transverse correlation functions and analyze their diffusive character. Conclusions are given in Sec. V.

II. THEORY

We define the CIMTF by the Hamiltonian

$$H=-\Omega\sum_i S_i^x-\frac{1}{2}\sum_{i,j}J_{ij}S_i^zS_j^z, \tag{1}$$

where $\vec{S}_i$ is a classical spin vector ($|\vec{S}_i|=1$) located at the lattice site i, Ω is a transverse field, and $J_{ij}=J$ is the longitudinal interaction acting between the nearest neighbors only. The equations of motion, which govern the dynamics of the model, are usually derived from the corresponding quantum-mechanical equations for the case of finite S,

$$\dot{\vec{S}}_i=(i/\hbar)[H,\vec{S}_i]_-. \tag{2}$$

After the variables have been properly rescaled and the commutators evaluted, the limit $S\to\infty$ is invoked and the operators are replaced by their c-number counterparts. It is nevertheless unnecessary to appeal to the limit of quantum results. Following Mermin,[12] the classical equations of motion can be written

$$\dot{S}_i^\alpha=\left(\vec{S}_i,\frac{\partial S_i^\alpha}{\partial\vec{S}_i},\frac{\partial H}{\partial\vec{S}_i}\right),\quad \alpha=x,y,z, \tag{3}$$

where $(\vec{a},\vec{b},\vec{c})=\vec{a}\cdot(\vec{b}\times\vec{c})$ denotes the mixed product. Hence,

$$\dot{S}_i^x=\sum_j J_{ij}S_j^zS_i^y, \tag{4a}$$

$$\dot{S}_i^y=-\sum_j J_{ij}S_j^zS_i^x+\Omega S_i^x, \tag{4b}$$

$$\dot{S}_i^z=-\Omega S_i^y. \tag{4c}$$

A convenient way to study the dynamics of the system is to look at the correlation functions

$$\tilde{C}^{\mu\nu}(\vec{q},t)=\langle\tilde{S}^\mu(-\vec{q},0)\tilde{S}^\nu(\vec{q},t)\rangle, \tag{5}$$

where $\tilde{S}^\mu(\vec{q},t)=S^\mu(\vec{q},t)-\langle S^\mu(\vec{q})\rangle$, $\langle\ \rangle$ denotes the thermodynamic average and

$$\vec{S}(\vec{q},t)=N^{-1/2}\sum_i e^{i\vec{q}\cdot\vec{R}_i}\vec{S}_i(t). \tag{6}$$

In addition, we introduce the normalized relaxation function and the relaxation shape function (RSF)

$$F^{\mu\nu}(\vec{q},t)=\tilde{C}^{\mu\nu}(\vec{q},t)/\tilde{C}^{\mu\nu}(\vec{q},0), \tag{7}$$

$$F^{\mu\nu}(\vec{q},\omega)=\frac{1}{2\pi}\int_{-\infty}^{\infty}dt e^{-i\omega t}F^{\mu\nu}(\vec{q},t). \tag{8}$$

Note that in Eq. (8) already a classical limit has been employed.

The theoretical approach, which provides the most systematic framework for the discussion of the IMTF dynamics, follows the continued-fraction analysis of the RSF, first introduced by Mori,[13]

$$F^{\alpha\alpha}(\vec{q},\omega)=\frac{1}{\pi}\,\mathrm{Re}\left\{\left[i\omega+\delta_{1\alpha}^{\vec{q}}\Big/\left(i\omega+\frac{\delta_{2\alpha}^{\vec{q}}}{i\omega+\cdots}\right)\right]^{-1}\right\}. \tag{9}$$

Here, $\delta_{1\alpha}^{\vec{q}},\delta_{2\alpha}^{\vec{q}},\ldots$ are related to the frequency moments of $F^{\alpha\alpha}(\vec{q},\omega)$,

$$\delta_{1\alpha}^{\vec{q}}=\langle\omega^2\rangle_{\vec{q}}^{\alpha\alpha}, \tag{10a}$$

$$\delta_{2\alpha}^{\vec{q}}=\langle\omega^4\rangle_{\vec{q}}^{\alpha\alpha}/\langle\omega^2\rangle_{\vec{q}}^{\alpha\alpha}-\langle\omega^2\rangle_{\vec{q}}^{\alpha\alpha}, \tag{10b}$$

where

$$\langle\omega^n\rangle_{\vec{q}}^{\alpha\alpha}=\int_{-\infty}^{\infty}d\omega F^{\alpha\alpha}(\vec{q},\omega)\omega^n. \tag{11}$$

The RSF representation as given by Eq. (9) becomes useful when the dynamics of the system is dominated by few slower processes with frequencies centered in the complex plane around $\omega=0$. When this is the case Eq. (9) may be truncated at a certain level whereby the effect of faster processes is taken into account via some real frequency-independent parameter λ.

In the present work we are able to evaluate frequency moments separately from our MC data[11] (or exactly at $T=\infty$), thus from Eqs. (10a) and (10b) also $\delta_{1\alpha}^{\vec{q}}$, $\delta_{2\alpha}^{\vec{q}}$. In this way we avoid any approximations at this stage. We list here few expressions relating lowest-order moments, which we will need later, to the static correlation

functions. Note that $\langle\omega^{2k+1}\rangle_{\vec{q}}^{\alpha\alpha}=0$:

$$\langle\omega^2\rangle_{\vec{q}}^{xx}=N^{-1}\times\sum_{\vec{k}}\frac{J_{\vec{k}}[\tilde{C}^{zz}(\vec{k},0)-\tilde{C}^{yy}(\vec{q}-\vec{k},0)]}{\beta\tilde{C}^{xx}(\vec{q},0)}\,, \tag{12}$$

$$\langle\omega^2\rangle_{\vec{q}}^{zz}=\langle S^x\rangle\Omega/\beta\tilde{C}^{zz}(\vec{q},0)\,, \tag{13}$$

$$\langle\omega^4\rangle_{\vec{q}}^{zz}=\langle\omega^2\rangle_{\vec{q}}^{zz}\left(\omega_{\vec{q}}^2+\frac{\Omega}{N\langle S^x\rangle}\times\sum_{\vec{k}}J_{\vec{k}}[\tilde{C}^{zz}(\vec{k},0)-\tilde{C}^{xx}(\vec{q}-\vec{k},0)]\right), \tag{14}$$

where $\beta=1/k_BT$ and

$$\omega_{\vec{q}}^2=\Omega^2-\Omega\langle S^x\rangle J_{\vec{q}}+(J_{\vec{q}=0}\langle S^z\rangle)^2\,, \tag{15}$$

$$J_{\vec{q}}=\sum_j J_{ij}\exp[-i\vec{q}\cdot(\vec{R}_i-\vec{R}_j)]\,. \tag{16}$$

Already $\langle\omega^6\rangle_{\vec{q}}^{zz}$ and $\langle\omega^4\rangle_{\vec{q}}^{xx}$ involve three- and four-spin correlation functions which are, even within the MC simulation, difficult to evaluate. Fortunately, in the case of the longitudinal RSF $F^{zz}(\vec{q},\omega)$ which is physically the most interesting, the three-pole truncation of Eq. (9) seems to be sufficient for a qualitative description of the IMTF spectra in the disordered phase,

$$F_3^{zz}(\vec{q},\omega)=\frac{1}{\pi}\frac{\lambda_{3z}^{\vec{q}}\delta_{1z}^{\vec{q}}\delta_{2z}^{\vec{q}}}{\omega^2(\omega^2-\delta_{1z}^{\vec{q}}-\delta_{2z}^{\vec{q}})^2+[\lambda_{3z}^{\vec{q}}(\omega^2-\delta_{1z}^{\vec{q}})]^2}\,. \tag{17}$$

(We henceforth omit indices z and $\vec{q}$ wherever there can be no ambiguity as to their meaning.) Theoretical evaluations of λ_3 have to rely on rather crude approximations. Lovesey and Meserve[14] assume a Gaussian time decay of the memory kernel in Eq. (9), which yields

$$\lambda_3^{\mathrm{LM}}=(\tfrac{1}{2}\pi\delta_2)^{1/2}. \tag{18}$$

Tommet and Huber[4] interpolate between Eq. (18), which seems to be justified in the critical regime with a well-pronounced central mode, and the expression more appropriate for a resonant behavior of $F^{zz}(\vec{q},\omega)$,

$$\lambda_3^{\mathrm{TH}}=\left(\frac{\pi}{2}\right)^{1/2}\left(\frac{\delta_2^{3/2}}{\delta_1+\delta_2}+\frac{0.5\delta_1^2\delta_2^{-1/2}}{\delta_1+\delta_2}\right). \tag{19}$$

Cheung[5] uses a mode-coupling approach to estimate λ_3. Whereas Eqs. (18) and (19) predict a finite value of $\lambda_3^{\vec{q}=0}$ at the transition temperature T_c, Cheung's result suggests a critical behavior of λ_3, namely, $\lambda_3^0\propto(T-T_c)^{1/2}$.

In the analysis of our MD data we shall employ also the two-pole approximation

$$F_2^{zz}(\vec{q},\omega)=\frac{1}{\pi}\frac{\lambda_2\delta_1}{(\omega^2-\delta_1)^2+\lambda_2^2\omega^2}\,, \tag{20}$$

where, in general, $\lambda_2\neq\lambda_3$. In contrast to the longitudinal RSF, neither $F_2^{xx}(\vec{q},\omega)$ nor $F_3^{xx}(\vec{q},\omega)$ would present a satisfactory approximation to the transverse RSF, which appear to be partly diffusive in character.

III. NUMERICAL-SIMULATION METHOD

Within our numerical-simulation approach we have studied the CIMTF on a 3-D simple cubic lattice with $N=16\times17\times18=4896$ spins. For convenience, the boundary conditions were taken to be staggered periodic. Our procedure was divided into two steps.[15] First, for a given temperature the MC technique was used, whereby the system was allowed to age 500–700 MC steps/spin, which insured a well-defined thermal equilibrium also with respect to large-distance static correlation functions $\tilde{C}^{\mu\nu}(\vec{R},0)$.[11] The final configuration thus obtained served as the initial condition for the MD procedure. While solving the system of Eqs. (4a)–(4c) we employed the fourth-order Runge-Kutta algorithm with a time increment typically $\frac{1}{20}$ mean-field-approximation (MFA) precession time, which proved to be sufficient to maintain the desired numerical accuracy. In the evaluation of $\tilde{C}^{\mu\nu}(\vec{R},t)$ we used the statistical significant sampling as proposed recently by Koehler and Lee,[16]

$$\tilde{C}^{\mu\nu}(\vec{R},t)=\frac{1}{N_mN_lN_{G'}}\times\sum_m^{N_m}\sum_l^{N_l}\sum_{G'}[\tilde{S}^{\mu}(\vec{R}_l,t_m)\tilde{S}^{\nu}(\vec{R}_l+G'\vec{R},t+t_m)]\,. \tag{21}$$

In Eq. (21), m runs only over uncorrelated time intervals where $t_m-t_{m-1}=\tau$ is determined by a characteristic decay time of the fluctuations within the system. In our calculations we have fixed τ by its $T=\infty$ value where it was approximately equal to one MFA precession period. The spatial summation takes into account only uncorrelated volumes; therefore $|\vec{R}_m-\vec{R}_{m-1}|\sim\kappa^{-1}$, κ being the inverse statical correlation length (in our examples correlated volumes contained 1, 8, 27 sites, respectively), while $G'\vec{R}$ generates the group of equivalent $\vec{R}$.

While calculating $F^{\mu\nu}(\vec{q},\omega)$ from $\tilde{C}^{\mu\nu}(\vec{R},t)$ we used the appropriate Gaussian filtering in the $\vec{q}$ as well as in the ω Fourier transforms[16] to avoid various termination effects and to suppress the data which were already below the thermal noise level.

IV. RESULTS AND DISCUSSION

The static and dynamic properties of the CIMTF are, for a given lattice, determined by two dimensionless parameters, the reduced transverse field $\gamma = \Omega/J$, and the reduced temperature $\eta = k_B T/J$. Note that $\gamma = 0$ corresponds to the ordinary $S = \infty$ Ising model. The effect of finite γ is reflected in the decrease of the critical η_c. When the value $\gamma = \gamma_c$ is reached, $\eta_c = 0$ and the phase transition is suppressed altogether. In Fig. 1 we present the phase diagram for the CIMTF on a simple cubic (sc) lattice, as calculated within the high-temperature-expansion approach.[11] For comparison we include also two points, accurately determined via the MC simulation, as well as curves representing MFA and self-consistent RPA results. It is worth noting that, in contrast to the $S = \frac{1}{2}$ case, $\gamma_c = J_{\vec{q}=0}^{-}/J$ is known exactly for the CIMTF, due to an entirely MFA behavior of the model at $T = 0$.

Since a MD study of the CIMTF within the whole range of both parameters was unfeasible, we restricted our calculations mainly to the $\gamma = \frac{1}{2}\gamma_c = 3$ case. There, the phase transition was located by the MC data at $\eta_c = 1.305$. One of our main aims was the investigation of the critical behavior of the longitudinal RSF. For this purpose we perfomed the MD simulation at $\eta = 1.25$, 1.35, 1.4, and 1.7. These temperatures are more or less all effectively in the critical regime, at least as far as the statical quantities are concerned. We were not able to approach η_c more closely, since the finite size effects would show up in the large-distance correlations, while at the same instant longer time sampling would be needed to average out the very slow critical fluctuations (mainly in $\langle S^z \rangle$). The $\eta = \infty$ case deserves the attention by its own, because it often represents the starting point for the extrapolations to lower temperatures, especially when the knowledge of parameters such as λ is lacking. Also, we are treating separately the transverse-relaxation functions.

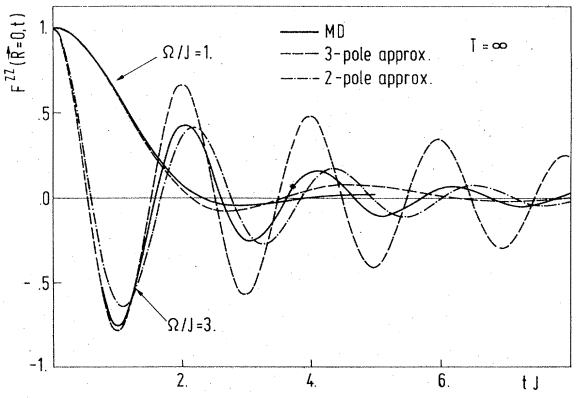

FIG. 2. $F^{zz}(\vec{R}=0,t)$ vs tJ at $T=\infty$ for two values of Ω/J. For comparison $F_2^{zz}(\vec{R}=0,t)$ and $F_3^{zz}(\vec{R}=0,t)$ with best adjusted λ are also plotted.

A. Longitudinal-relaxation functions: $T = \infty$

The longitudinal-relaxation functions reduce at $\eta = \infty$ to $F^{zz}(\vec{q},t) = 3\tilde{C}^{zz}(\vec{R}=0,t)$ and are thus $\vec{q}$ independent. In Fig. 2 we plot our MD result for $F^{zz}(\vec{R}=0,t)$. Besides the $\gamma = 3$ case, we include here also the $\gamma = 1$ case, where the value of γ corresponds more closely to the experimental situation in pure KDP. At $\gamma = 1$ $F^{zz}(\vec{R}=0,t)$ in Fig. 2 clearly exhibits an overdamped character, whereas for $\gamma = 3$ we observe damped oscillations with an effective frequency approximately equal to Ω. The same behavior can be traced in the $F^{zz}(\vec{R}=0,\omega)$ spectra shown in Fig. 3.

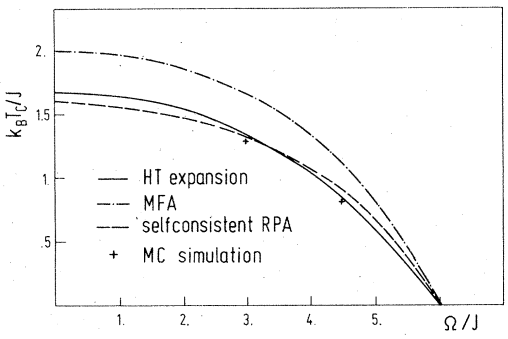

FIG. 1. Phase diagram of the CIMTF on a sc lattice, i.e., $k_B T_c/J$ plotted vs Ω/J, as obtained by the high-temperature expansion to the fifth order (Ref. 11). The MFA and self-consistent RPA curves are also presented. Crosses denote MC simulation results.

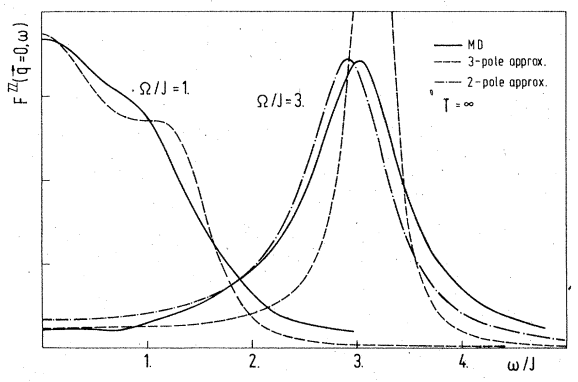

FIG. 3. $F^{zz}(\vec{R}=0,\omega)$ vs ω/J at $T=\infty$ for two values of Ω/J. $F_2^{zz}(\vec{R}=0,\omega)$ and $F_3^{zz}(\vec{R}=0,\omega)$ are plotted with the same parameters as in Fig. 2.

The resonant spectra, as realized for the $\gamma = 3$ case, are usually described in terms of two displaced Lorentzians, centered at ω_0 and $-\omega_0$, where $\omega_0 \sim \Omega$. However, this form lends a satisfactory representation of the observed curve only for $|\omega - \omega_0|\tau < 1$, τ being a characteristic decay time. First, the Lorentzian curve clearly fails at higher ω due to the moment violation; $\langle\omega^n\rangle = \infty$ for $n > 2$. Moreover, it cannot properly take into account the marked asymmetry of the spectral line. Both these deficiencies are partly eliminated within the two-pole and three-pole approximations, Eqs. (17) and (20). To investigate the feasibility of both representations at $\gamma = 3$, we applied a best-fit procedure for λ_2 and λ_3, respectively, whereas $\delta_1 = \Omega^2$ and $\delta_2 = 2J^2$ are known exactly at $\eta = \infty$. The corresponding curves are also included in Figs. 2 and 3, where $\lambda_2 = 1.21J$ and $\lambda_3 = 2.6J$.

It can be easily observed that $F^{zz}(\vec{R}=0, t)$ for $\gamma = 3$ does not follow a simple $\cos\Omega t\, e^{-t/\tau}$ law. A well-defined $\tau = 1.12/J$ is established only for $t > 2/J$, while the damping estimated from the first-oscillation period would yield a much larger value, $\tau = 1.67/J$. $F_3^{zz}(\vec{R}=0, t)$, as obtained by an analytical transformation of Eq. (17),[14] is a very accurate approximation for $t < 1.5/J$ (rather λ_3 independent). However, the fixed form of the first period induces, for larger times, oscillations with markedly underestimated damping. On the other hand, $F_2^{zz}(\vec{R}=0, t)$ fits satisfactorily the overall behavior at the expense of a badly reproduced first period and some phase shift in later periods. Similar conclusions can be reached from the spectra in Fig. 3. $F^{zz}(\vec{R}=0, \omega)$ is centered at $\omega_p = 3.06J$. The two-pole approximation provides $\omega_{2p} = 2.87J$, whereby the shift is caused by the wings which fall less rapidly than our MD curve. Nevertheless, $F_2^{zz}(\vec{R}=0, \omega)$ accounts properly for the observed line shape. At the same time $F_3^{zz}(\vec{R}=0, \omega)$ fails completely in width as well as in peak position. Namely, from Eq. (17) it follows that the two-peak structure of the spectra is recovered only for $\lambda_3 \geq \lambda_{3c} = (\delta_1 + \delta_2)/(2\delta_1)^{1/2}$, which in our case leads to $\lambda_{3c} = 2.59J$. This value is already much too large to reproduce correctly the width of the MD spectra. In this connection we can quote also the values, as obtained from Eqs. (18) and (19), $\lambda_3^{\mathrm{LM}} = 1.77J$ and $\lambda_3^{\mathrm{TH}} = 3.98J$. Although the latter expression was designed to cope with the double-peak spectra, it is easy to recognize that both λ_3 lead to an even worse representation of the MD data than the $F_3^{zz}(\vec{R}=0, \omega)$ plotted in Fig. 3. The apparent failure of the three-pole approximation in this case might be understood along the lines already discussed by Mori.[13] The use of n-pole approximations is legitimate only insofar that there are n poles of $F^{\alpha\alpha}(\vec{q}, \omega)$ located within $|z| < \omega_0$, the rest of them being well separated from this region. If this condition is not met we may obtain unprecise results when retaining only first n poles.

Turning now to the $\gamma = 1$ case, it becomes clear that $F_2^{zz}(\vec{R}=0, \omega)$ fails whereas $F_3^{zz}(\vec{R}=0, \omega)$ at least qualitatively accounts for the merging of the overdamped mode with the nascent central component. Also, the fitted $\lambda_3 = 1.59J$ overlaps to great extent with the theoretically predicted values, $\lambda_3^{\mathrm{LM}} = 1.77J$ and $\lambda_3^{\mathrm{TH}} = 1.33J$.

B. Longitudinal-relaxation functions: finite T

As we lower the temperature, more distant correlations become important. In Fig. 4 different relaxation functions $F^{zz}(\vec{R}, t)$ are plotted for $\eta = 1.35$ just above the phase transition $\eta_c = 1.305$. At short times the curves for $R > 0$ reveal an extended plateau, which is due to the fact that the lowest moments are exactly zero for large-distance $F^{zz}(\vec{R}, \omega)$, namely, $\langle\omega^2\rangle_{\vec{R}}^{zz} = 0$ for $R > 0$, $\langle\omega^4\rangle_{\vec{R}}^{zz} = 0$ for $R > a_0$, a_0 denoting the lattice spacing, etc. The long-time behavior is characterized by common damped oscillations, their period being determined for all $\vec{R}$ by an average soft-mode frequency, which are superimposed on a slow relaxational process. The contributions of $R > a_0$ functions are essential in the low-frequency regime near η_c. For $q > \pi\kappa$ their influence is less dramatic since the $\vec{q}$ transformation tends to average them out. On the other hand, at $q < \pi\kappa$ as many functions as possible should be included in the evaluation of $F^{zz}(\vec{q}, t)$. To this purpose, we calculated in the present examples up to 35 nonequivalent $C^{zz}(\vec{R}, t)$ via Eq. (21), i.e., from $\vec{R}=0$ to $\vec{R}=(4,4,0)a_0$. This was necessitated by the fact that in the most critical example ($\eta = 1.35$) $\kappa^{-1} \sim 3.5a_0$ and also $R > 5a_0$

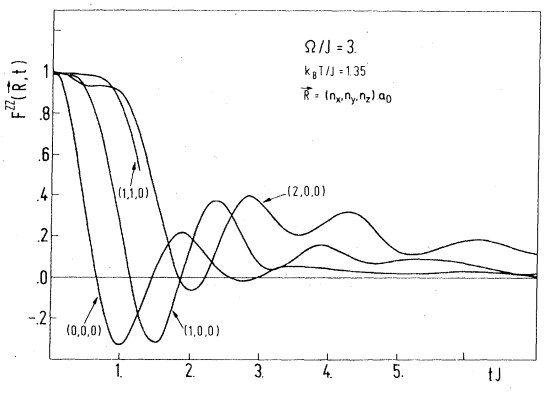

FIG. 4. $F^{zz}(\vec{R}, t)$ vs tJ at $\eta = k_B T/J = 1.35$ just above the critical point $\eta_c = 1.305$ for $\Omega/J = 3$ and various nonequivalent $\vec{R}$.

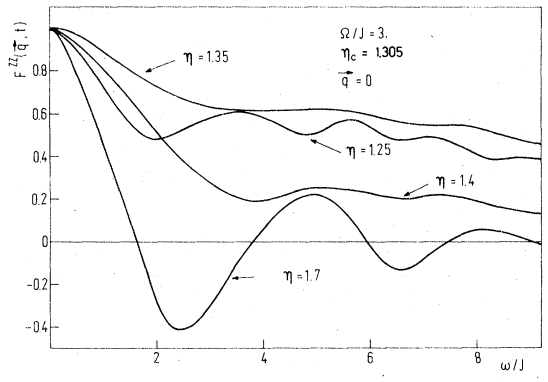

FIG. 5. $F^{zz}(\vec{q}=0,t)$ vs tJ at $\Omega/J=3$ for various $\eta=k_BT/J$. Note that $\eta=1.25<\eta_c$ corresponds to the ordered phase.

had to be considered in order to achieve a reasonable q resolution.

In Fig. 5 we present the results for $F^{zz}(\vec{q}=0,t)$ at different η in the critical regime (the $\eta=1.7$ case is effectively outside this regime since $\kappa^{-1}\sim a_0$). Whereas the $\eta=1.7$ curve still retains the qualitative character of the $\eta=\infty$ case in Fig. 2, at $\eta=1.4$ the oscillating part of $F^{zz}(\vec{q}=0,t)$ is already less important, and the process is dominated by the critical-slowing-down phenomenon. This trend is even more pronounced for $\eta=1.35$ where the amplitude of the superimposed oscillations is further diminished. In the $\eta=1.25$ case which, in contrast to all preceding examples, represents the situation in the ordered phase $\eta<\eta_c$, the oscillations become enhanced again. It must

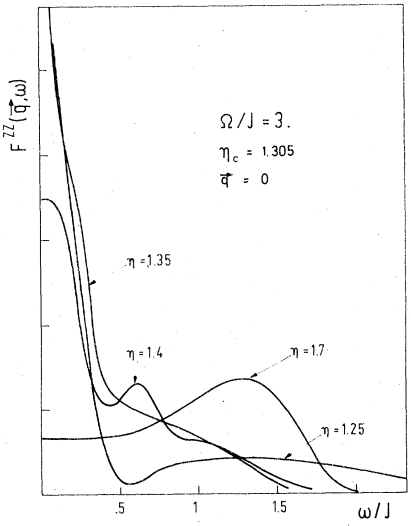

FIG. 6. $F^{zz}(\vec{q}=0,\omega)$ vs ω/J at $\Omega/J=3$ for different temperatures $\eta=k_BT/J$.

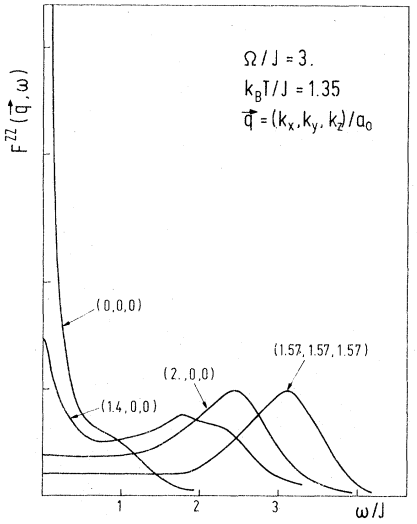

FIG. 7. $F^{zz}(\vec{q},\omega)$ vs ω/J at $\eta=k_BT/J=1.35$ just above the critical η_c for $\Omega/J=3$ and different $\vec{q}$ in the Brillouin zone.

be noted that, due to $\langle S^z\rangle\neq 0$, the physical interpretation here is slightly different, thus attributing the slow decaying part of $F^{zz}(\vec{q}=0,t)$ to the conventional longitudinal relaxation of $\langle S^z\rangle$, which persists also outside the critical regime. The behavior described above is reflected also in the spectra $F^{zz}(\vec{q}=0,\omega)$ in Fig. 6. At $\eta=1.7$ only a damped soft mode can be observed, whereas in the $\eta=1.4$ case besides the soft-mode component a strong central mode emerges. It is worthwhile pointing out the structure of the soft-mode component which indicates a slightly narrower peak on the otherwise overdamped background. This was achieved while improving the q resolution over the preliminary version.[17] The $\eta=1.35$ case is dominated by the central mode while the soft mode is overdamped. Again, $\eta=1.25$ is quite different in character, allowing the existence of an underdamped soft mode besides a narrow central peak.

In Fig. 7 we present the spectra $F^{zz}(\vec{q},\omega)$ for a fixed temperature $\eta=1.35$, but for various $\vec{q}$ in the Brillouin zone. At $q>q_0\sim 1.7/a_0$ the spectra reveal resonances at $\omega_p\sim\pm\omega_{\vec{q}}$, where $\omega_{\vec{q}}$'s correspond to the RPA frequencies in Eq. (15). The same behavior appears for $\eta=1.4$ at $q>1.5/J$ while in the $\eta=1.7$ case it is characteristic for all $\vec{q}$ (see Fig. 6). At $q<q_0$ the central mode at $\omega=0$ begins to emerge. At the same time the soft mode becomes increasingly damped and for $q\sim 0$ finally disappears into the central component. The value of q_0 to great extent coincides with $q_0\sim\pi\kappa$, which confirms our previous discussion.

We can now test our results on two conditions, mentioned in Sec. I, which $F^{zz}(\vec{q},\omega)$ should satisfy

TABLE I. Values of the parameters $\delta_1^{\vec{q}}$, $\delta_2^{\vec{q}}$, $\lambda_3^{\vec{q}}$ for $\vec{q}=0$ at various temperatures η in the paraphase, as obtained by the MC simulation—δ_1^0, δ_2^0, by the three-parameter fit of $F^{zz}(\vec{q}=0,t)$—$\delta_1^{0f}, \delta_2^{0f}$, λ_3^{0f}, by the one-parameter fit of $F^{zz}(\vec{q}=0,t)$—λ_3^{0p}, from the height $F^{zz}(\vec{q}=0,\omega=0)$—$\lambda_3^{0h}$, and from the expressions (18) and (19)—$\lambda_3^{0\,\mathrm{LM}}$, $\lambda_3^{0\,\mathrm{TH}}$, respectively.

	δ_1^0/J^2	δ_2^0/J^2	δ_1^{0f}/J^2	δ_2^{0f}/J^2	λ_3^{0p}/J	λ_3^{0f}/J	λ_3^{0h}/J	$\lambda_3^{0\,\mathrm{LM}}/J$	$\lambda_3^{0\,\mathrm{TH}}/J$
∞	9	2	...	...	2.6	...	3.3	1.77	3.98
1.7	1.00	1.73	1.31	1.30	1.8	1.64	2.	1.65	1.22
1.4	0.39	1.48	0.36	1.15	1.07	0.90	0.8	1.52	1.25
1.35	0.18	2.04	0.20	1.35	0.80	0.51	0.75	1.79	1.65
1.305	0.0	2.80						2.10	2.10

in order that their central component might be attributed to propagating domain walls: (a) Clearly, none of the presented examples supports strongly the notion that the central- and the soft-mode component could coexist well separated, which would be an indication of the existence of two kinds of approximately independent processes. We may conclude from Figs. 5–7 that the soft mode remains underdamped (but still heavily damped) in the presence of the central mode only in a narrow region of η and $\vec{q}$ (i.e., $q=0$, $\eta\sim 1.4$ and $\eta=1.35$, $q\sim 1.4/a_0$). (b) A check on the propagating character of the central mode would be a phononlike structure of the central peak for small q. Thus $F^{zz}(\vec{q},\omega)$ would reach a maximum value at $\omega_p\sim c_0 q$ and c_0 would be related to the effective domain-wall velocity. In our $\eta=1.35$ case the height of the central peak decreases as $(qa_0)^2$ and no new off-center maxima are observed. For $\eta=1.4$ the conclusions are somewhat less certain. Having in mind our q resolution, $\Delta q\sim 0.25/a_0$, as well as the frequency resolution, $\Delta\omega\sim 0.07J$, we can note that the peak width in Fig. 7 is considerably larger while the top of the peak is rather flat. These facts indicate some possible structure which however could not be resolved within our accuracy. Nevertheless, it still seems plausible from the analogy with the lattice-dynamical model[6] that the central mode might be connected with a cluster dynamics, although this dynamics does not possess a propagating character.

Finally, let us turn to a continued-fraction analysis of the $F^{zz}(\vec{q},\omega)$ spectra. For the examples in Figs. 6 and 7 which do not involve a central component, the two-pole representation as given by Eq. (20) is generally more appropriate. We do not repeat here the discussion presented in this connection in Sec. IV A. Concentrating predominantly on the examples incorporating the central mode, we can state that the three-pole approximation (17) becomes increasingly reliable as we approach η_c. In order to get a quantitative understanding of the most interesting $q=0$ situation, we performed three independent fitting procedures within $F_3^{zz}(\vec{q}=0,\omega)$ to estimate λ_3^0, which reproduce the best agreement with our MD RSF:

(a) First, $F^{zz}(\vec{q}=0,t)$ curves as presented in Fig. 5 were fitted to $F_3^{zz}(\vec{q}=0,t)$,[14] where only the λ_3^0's were taken to be unknown parameters. The remaining δ_1^0 and δ_2^0 were obtained from Eqs. (10a), (10b), (13), and (14), where for $\langle S^x\rangle$, $\tilde{C}^{zz}(\vec{q},0)$, and $\tilde{C}^{xx}(\vec{q},0)$ the MC data were used.[11] The frequency moments could as well have been deduced from the short-time behavior

$$F^{zz}(\vec{q},t)=1-\tfrac{1}{2}\langle\omega^2\rangle_{\vec{q}}^{zz}t^2+\tfrac{1}{24}\langle\omega^4\rangle_{\vec{q}}^{zz}t^4-\cdots. \qquad (22)$$

However, the straightforward application of Eq. (22) to the evaluation of $\langle\omega^n\rangle_{\vec{q}}^{zz}$ is not practicable at $n>2$ and could lead to ambiguous results.

To understand the behavior of δ_1^0, δ_2^0, and λ_3^0 near η_c, we must quote here a few results obtained via the MC simulation.[11] $\langle S^x\rangle$ is a monotonous function of η for $\eta>\eta_c$. The same is true for $\tilde{C}^{yy}(\vec{q},0)=\langle S^x\rangle/\beta\Omega$, which is exactly $\vec{q}$ independent, and $\tilde{C}^{xx}(\vec{q},0)$. $\tilde{C}^{xx}(\vec{q},0)$ appears to be for $\gamma=3$ almost identical to $\tilde{C}^{xx}(\vec{R}=0,0)$ in the whole range of η, where more distant correlations contribute corrections below 1%. The critical behavior of $\delta_1^{\vec{q}}$ is thus, via Eq. (13), determined by $\tilde{C}^{zz}(\vec{q},0)$. On the other hand, we can show by the use of Eqs. (10b) and (14) that in the vicinity of η_c $\delta_2^{\vec{q}}$ is dominated by the $\tilde{C}^{zz}(\vec{R}_{nn},0)$ term, where $\vec{R}_{nn}=(1,0,0)a_0$. δ_2^0 thus exhibits a cusplike dependence $\delta_{2c}^0-\delta_2^0\propto|T-T_c|^{\nu}$, ν denoting the correlation-length critical exponent ($\nu\simeq\frac{2}{3}$ in a 3-D lattice).

The values for δ_3^{0p} obtained by the one-parameter fit procedure are given in Table I, together with corresponding δ_1^0 and δ_2^0. The matching of the calculated $F_3^{zz}(\vec{q}=0,t)$ with the MD curves is not very satisfactory since the oscillations dephase after 1.5–2 cycles. Also, the $F_3^{zz}(\vec{q}=0,\omega)$ spectra show a general tendency to underplay the width of the soft mode.

(b) To overcome these two difficulties we have performed also a three-parameter fit with respect to δ_1^0, δ_2^0, and λ_3^0 to obtain an $F_3^{zz}(\vec{q}=0,t)$ which would achieve an overall agreement with the MD

data. The corresponding δ_1^{0f}, δ_2^{0f}, and λ_3^{0f} are presented in Table I. Note that δ_1^{0f} still largely agrees with the exact δ_1^0, whereas the δ_2^{0f}'s are essentially lower than δ_2^0.

(c) Finally, λ_3^0 has been determined from the height of the spectra at $\omega=0$, where Eq. (17) yields

$$\lambda_3^{0h}=\delta_2^0/\pi\delta_1^0 F^{zz}(\vec{q}=0,\omega=0)\,, \tag{23}$$

For δ_1^0 and δ_2^0 in Eq. (23) we again insert the MC values.

All three sets of λ_3^0 values in Table I are reasonably consistent and they exhibit a common trend, i.e., they decrease as η_c is approached from above. The results also indicate that λ_3 is less critical than δ_1, which is essential for an approximate validity of the conventional critical-dynamics theory.[10] The disagreement between the fitted λ_3^0 values and the theoretical estimations $\lambda_3^{0\mathrm{LM}}$, $\lambda_3^{0\mathrm{TH}}$ (note that $\lambda_3^{0\mathrm{LM}}=\lambda_3^{0\mathrm{TH}}$ at $\eta=\eta_c$) is not so large as one would expect from the crude approximations which were applied while deriving Eqs. (18) and (19). Nevertheless, the theoretical values reveal, besides the discussed deficiency at $\eta\gg\eta_c$, an essentially different trend in the critical regime. Cheung[5] evaluated λ_3^0 within the model coupling approach. Replacing in the critical regime $F^{zz}(\vec{q},t)$ by $F_3^{zz}(\vec{q},t)$ and taking into account only the diffusive part of $F^{xx}(\vec{q},t)$ [see Eq. (24)], he obtained a critical dependence $\lambda_3^0\propto C^{-1}$, where C denotes the specific heat. Thus, $\lambda_3^0\propto|T-T_c|^{1/8}$, which induces a qualitatively similar behavior to that observed in our MD simulation. However, the approach involved many questionable approximations and the estimated values are at least an order of magnitude too large.

C. Transverse-relaxation functions

According to the theory,[5] the transverse RSF $F^{xx}(\vec{q},\omega)$ can be for small $\vec{q}$ and ω written

$$F^{xx}(\vec{q},\omega)=\frac{1}{\pi}\frac{\chi_T^{xx}-\chi_S^{xx}}{\chi_T^{xx}}\frac{D_E q^2}{\omega^2+(D_E q^2)^2}+g(\omega)\,. \tag{24}$$

Here, D_E is the diffusion constant for the energy density, χ_T^{xx} and χ_S^{xx} are the isothermal and the adiabatic susceptibilities, respectively, while $g(\omega)$ is supposed to be a slowly varying function of $\vec{q}$ and ω. The first term in Eq. (24) represents the diffusion of the transverse spin components which should persist for all $\eta>\eta_c$. In order to check up on the diffusive character of the transverse relaxation functions we calculated, for $\gamma=3$ and $\eta=\infty, 1.35$, 20 nonequivalent $\tilde{C}^{xx}(\vec{R},t)$. Few lowest ones, multiplied by their symmetry factors $Z_{\vec{R}}$, are plotted in Figs. 8 and 9. It can be clearly seen that the functions display features

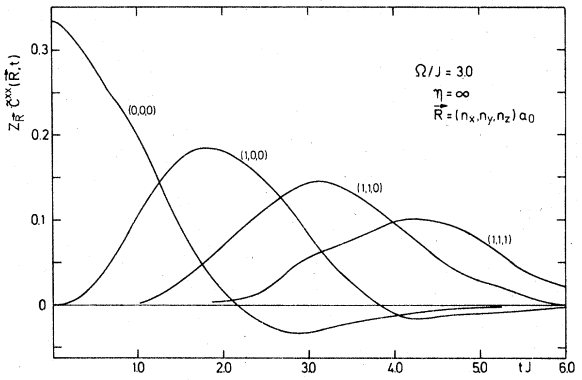

FIG. 8. Few lowest $\tilde{C}^{xx}(\vec{R},t)$, multiplied by their symmetry factors in a sc lattice $Z_{\vec{R}}$, plotted vs tJ at $\eta=\infty$.

pertinent to the diffusion processes. The only deviations are observed at short times in the diagonal $\tilde{C}^{xx}(\vec{R}=0,t)$ which is entirely consistent with Eq. (24) where $g(\omega)$ accounts for this effect. The relative intensity of the diffusive part ζ_D within $F^{xx}(\vec{q},\omega)$ can be calculated via the relation[5]

$$\zeta_D=\frac{\chi_T^{xx}-\chi_S^{xx}}{\chi_T^{xx}}=-\left(\frac{\partial\langle S^x\rangle}{\partial\beta}\right)^2\Big/\frac{\partial\langle H\rangle}{\partial\beta}\,\tilde{C}^{xx}(\vec{q}=0,0)\,. \tag{25}$$

At $\eta=\infty$, Eq. (25) simplifies within the sc lattice to

$$\zeta_D=\Omega^2/(\Omega^2+J^2)\,. \tag{26}$$

For $\gamma=3$ we obtain $\zeta_D=0.9$, whereas for $\eta=1.35$ we can deduce from our MC data using Eq. (25) $\zeta_D=0.27$. The $\eta=\infty$ case is thus almost entirely of a diffusive character. ζ_D diminishes while approaching η_c and following Eq. (25) vanishes, $\zeta_D\propto C^{-1}$. The short-time behavior of $\tilde{C}^{xx}(\vec{R}=0,t)$ in Figs. 8 and 9 can be understood with the help of frequency moments. It follows from Eq. (12) that

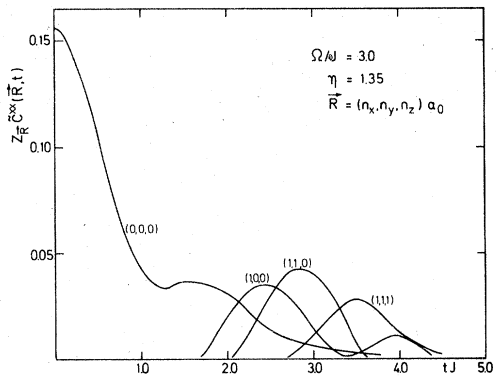

FIG. 9. Few lowest $\tilde{C}^{xx}(\vec{R},t)$, multiplied by their symmetry factors $Z_{\vec{R}}$, plotted vs tJ at $\eta=1.35$ just above η_c.

$\langle\omega^2\rangle_{\vec{q}}^{xx} = J_{\vec{q}=0}\tilde{C}^{zz}(\vec{R}_{nn},0)/\beta\tilde{C}^{xx}(\vec{q},0)$. The value at $\eta=\infty$ can be expressed exactly, $\langle\omega^2\rangle_{\vec{q}}^{xx} = 2J^2$, whereas for $\eta=1.35$ we use our MC data, $\langle\omega^2\rangle_{\vec{q}}^{xx} = 4.62J^2$. These rather large values indicate that the spectra $F^{xx}(\vec{q},\omega)$ incorporate, besides a narrow diffusive component, also extensive wings.

To give a quantitative estimate of D_E we employ the diffusion relation

$$D_E = \frac{1}{6}\, d\left[\left(\sum_j R_{ij}^2 \tilde{C}^{xx}(\vec{R}_{ij},t)\right) \Big/ \left(\sum_j \tilde{C}^{xx}(\vec{R}_{ij},t)\right)\right] \Big/ dt . \tag{27}$$

At $\eta=\infty$, Eq. (27) yields a well-defined value $D_E = 0.30Ja_0^2$ for $t>\tau=1/J$. τ indicates the decay time of $g(t)$ in Eq. (24) and is approximately related to the decay time of $\tilde{C}^{xx}(\vec{R}=0,t)$. We may compare this result with the theoretical estimate at $\eta=\infty$, which assumes a Gaussian decay of the energy-energy correlation function[18]

$$D_E^{\mathrm{TH}} = \lim_{\vec{q}\to 0} \frac{1}{q^2}\left(\frac{\pi(\langle\omega^2\rangle_{\vec{q}}^{EE})^3}{2\langle\omega^4\rangle_{\vec{q}}^{EE}}\right)^{1/2} = \frac{1}{6}\left(\frac{5\pi}{14}\right)^{1/2}\frac{\Omega^2}{\Omega^2+J^2}\,Ja_0^2 . \tag{28}$$

Note that in the derivation of Eq. (28) we already employed the $S=\infty$ limit. In our case Eq. (28) gives a smaller value, $D_E^{\mathrm{TH}} = 0.16Ja_0^2$. At $\eta=1.35$ an analysis via Eq. (27) is rather ambiguous due to the fact that the $\tilde{C}^{xx}(\vec{R},t)$ for $R>2a_0$ remain at all t below the 0.001 level and are dominated by the thermal noise. In spite of that we are able to deduce D_E accurately enough by comparing the time scales of diffusion in Figs. 8 and 9. The result $D_E = 0.80Ja_0^2$ indicates a much faster diffusion in the critical regime. Here, we can comment also on Cheung's result for D_E which he obtains by applying a mode-coupling approximation to the energy-energy correlation function,[5]

$$D_E \approx \frac{k_B\beta^2}{2CN}\sum_{\vec{q}'}\left|\frac{\vec{q}\cdot\nabla J_{\vec{q}'}}{q}\right|^2 \times \int_0^\infty [\dot{\tilde{C}}^{zz}(\vec{q}',t)]^2\,dt , \tag{29}$$

To evaluate Eq. (29) at $\eta=\infty$, we insert $\tilde{C}^{zz}(\vec{q}',t) \approx \frac{1}{3}F_2^{zz}(\vec{R}=0,t)$. Assuming also $\lambda_{2z}^2 \ll \delta_1$, we get $D_E = J^2a_0^2/3\lambda_{2z} = 0.27Ja_0^2$ which is in satisfactory agreement with our MD value. Near η_c the consistence of Eq. (29) with our MD result appears to be more questionable. As $\tilde{C}^{zz}(\vec{q}',t)$ does not incorporate the critical-slowing-down part, and furthermore small $\vec{q}'$ values are filtered out by the factor $(\vec{q}\cdot\nabla J_{\vec{q}'})^2$, the critical behavior would be determined by $D_E \propto C^{-1} \propto |T-T_c|^{1/8}$. An approximate evaluation of Eq. (29) for the $\eta=1.35$ case shows, however, that it can to some extent explain the rather large value of D_E, obtained from our MD data. A decrease of D_E could be expected only in the very vicinity of η_c.

V. CONCLUSIONS

Using the MD simulation approach we have studied the dynamics of the CIMTF on a 3-D sc lattice. In the critical regime above the phase transition our longitudinal RSF reveal the existence of the central mode, in addition to the conventional damped soft mode. We do not observe any new excitation branch in the low-frequency regime, which could be attributed, following the analogy with the lattice-dynamical model for the structural phase transitions, to the propagating domain walls. A physical explanation seems to be much heavier damping effects in the CIMTF which destroy the independence of soft modes and cluster modes. These arguments do not exclude the possibility of finding this phenomenon in other dimensionalities or in connection with a longer-range J_{ij}, which would depress the damping of the modes.

An analysis of our longitudinal RSF via the continued-fraction expansion shows that resonant-type spectra are well represented by a two-pole approximation. On the other hand, the three-pole representation has in these situations a tendency either to produce some ghost central peak or to underestimate badly the width of the spectral lines. In the critical regime the 3-pole approximation to $F^{zz}(\vec{q}=0,\omega)$ becomes increasingly reliable. Our MD data favor a decreasing trend of λ_3^0 when η_c is approached from the disordered phase. Our results for the transverse functions confirm their diffusive character. Lowering the temperature we observe a decrease in the intensity of the diffusive part, whereas D_E shows an opposite trend.

ACKNOWLEDGMENT

This work was supported by a grant from the Research Community of Slovenia.

*Permanent address: Dept. of Physics and Institute Jožef Stefan, University of Ljubljana, 61001 Ljubljana, Yugoslavia.

[1] R. B. Stinchcombe, J. Phys. C 6, 2459 (1973).

[2] D. P. Chock and R. Dagonnier, Physica (Utr.) 53, 393 (1971).

[3] M. A. Moore and H. C. W. L. Williams, J. Phys. C 5, 3185 (1972).

[4]T. N. Tommet and D. L. Huber, Phys. Rev. B 11, 1971 (1975).
[5]T. H. Cheung, Z. Phys. 267, 251 (1974).
[6]T. Schneider and E. Stoll, Phys. Rev. B 13, 1216 (1976).
[7]P. Pfeuty, J. Phys. C 9, 3993 (1976).
[8]R. A. Tahir-Kheli and D. G. Mc Fadden, Phys. Rev. 182, 604 (1969).
[9]H. E. Stanley, *Introduction to Phase Transitions and Critical Phenomena* (Oxford U.P., Oxford, 1971).
[10]P. C. Hohenberg and B. I. Halperin, Rev. Mod. Phys. 49, 435 (1977).
[11]P. Prelovšek and I. Sega, J. Phys. C 11, 2103 (1978).
[12]N. D. Mermin, J. Math. Phys. 8, 1061 (1967).
[13]H. Mori, Prog. Theor. Phys. 34, 399 (1965).
[14]S. W. Lovesey and R. A. Meserve, J. Phys. C 6, 79 (1973).
[15]R. E. Watson, M. Blume, and G. H. Vineyard, Phys. Rev. 181, 811 (1969).
[16]T. R. Koehler and P. A. Lee, J. Comp. Phys. 22, 319 (1976).
[17]P. Prelovšek and I. Sega, Proceedings of the International Conference on Lattice Dynamics, Paris, 1977 (unpublished).
[18]T. N. Tommet, thesis (University of Wisconsin, 1974) (unpublished). See also, D. L. Huber and T. Tommet, Solid State Commun. 12, 803 (1975).